

Winter Targeted Observing Periods during the Year of Polar Prediction in the Southern Hemisphere (YOPP-SH)

David H. Bromwich^{1b,a}, Irina V. Gorodetskaya^{b,c}, Scott Carpentier^d, Simon Alexander^e, Eric Bazile^f, Victoria J. Heinrich^g, Francois Massonnet^h, Jordan G. Powersⁱ, Jorge F. Carrasco^j, Arthur Cayette^k, Taejin Choi^l, Anastasiia Chyhareva^{m,n}, Steven R. Colwell^o, Jason M. Cordeira^p, Raul R. Cordero^q, Alexis Doerenbecher^f, Claudio Durán-Alarcón^b, W. John R. French^e, Sergi Gonzalez-Herrero^{r,bb}, Adrien Guyot^d, Thomas Haiden^s, Naohiko Hirasawa^t, Paola Rodriguez Imazio^u, Brian Kawzenuk^p, Svitlana Krakovska^{m,n}, Matthew A. Lazzara^v, Mariana Fontolan Litell^a, Kevin W. Manningⁱ, Kimberley Norris^g, Sang-Jong Park^l, F. Martin Ralph^p, Penny M. Rowe^w, Qizhen Sun^x, Vito Vitale^y, Jonathan D. Wille^{z,aa}, Zhenhai Zhang^p and Xun Zou^p

KEYWORDS:

Antarctica;
Southern Ocean;
Numerical weather prediction/
forecasting;
Cloud microphysics;
Numerical analysis/
modeling

ABSTRACT: The Year of Polar Prediction in the Southern Hemisphere (YOPP-SH) held seven targeted observing periods (TOPs) during the 2022 austral winter to enhance atmospheric predictability over the Southern Ocean and Antarctica. The TOPs of 5–10-day duration each featured the release of additional radiosonde balloons, more than doubling the routine sounding program at the 24 participating stations run by 14 nations, together with process-oriented observations at selected sites. These extra sounding data are evaluated for their impact on forecast skill via data denial experiments with the goal of refining the observing system to improve numerical weather prediction for winter conditions. Extensive observations focusing on clouds and precipitation primarily during atmospheric river (AR) events are being applied to refine model microphysical parameterizations for the ubiquitous mixed-phase clouds that frequently impact coastal Antarctica. Process studies are being facilitated by high-time-resolution series of observations and forecast model output via the YOPP Model Intercomparison and Improvement Project (YOPPsiteMIIP). Parallel investigations are broadening the scope and impact of the YOPP-SH winter TOPs. Studies of the Antarctic tourist industry's use of weather services show the scope for much greater awareness of the availability of forecast products and the skill they exhibit. The Sea Ice Prediction Network South (SIPN South) analysis of predictions of the sea ice growth period reveals that the forecast skill is superior to the sea ice retreat phase.

DOI: 10.1175/BAMS-D-22-0249.1

Corresponding author: David H. Bromwich, bromwich.1@osu.edu

Manuscript received 7 November 2022, in final form 19 June 2024, accepted 6 July 2024

© 2024 American Meteorological Society. This published article is licensed under the terms of the default AMS reuse license. For information regarding reuse of this content and general copyright information, consult the AMS Copyright Policy (www.ametsoc.org/PUBSReuseLicenses).

AFFILIATION: ^a Byrd Polar and Climate Research Center, The Ohio State University, Columbus, Ohio; ^b Interdisciplinary Centre of Marine and Environmental Research, University of Porto, Porto, Portugal; ^c Department of Physics, Centre for Environmental and Marine Studies, University of Aveiro, Aveiro, Portugal; ^d Bureau of Meteorology, Hobart/Melbourne, Australia; ^e Australian Antarctic Division, Kingston, Tasmania, Australia; ^f National Center for Meteorological Research, Meteo-France, Toulouse, France; ^g School of Psychological Sciences, University of Tasmania, Hobart, Tasmania, Australia; ^h Université catholique de Louvain, Louvain-la-Neuve, Belgium; ⁱ NSF/National Center for Atmospheric Research, Boulder, Colorado; ^j University of Magallanes, Punta Arenas, Chile; ^k Naval Information Warfare Center, Atlantic, Polar Programs IPT, Charleston, South Carolina; ^l Korea Polar Research Institute, Incheon, South Korea; ^m National Antarctic Scientific Center, Kyiv, Ukraine; ⁿ Ukrainian Hydrometeorological Institute, Kyiv, Ukraine; ^o British Antarctic Survey, Cambridge, United Kingdom; ^p Center for Western Weather and Water Extremes, Scripps Institution of Oceanography, University of San Diego, San Diego, California; ^q University of Santiago, Santiago, Chile; ^r Agencia Estatal de Meteorología, Barcelona, Spain; ^s European Centre for Medium-Range Weather Forecasts, Reading, United Kingdom; ^t National Institute of Polar Research, Tokyo, Japan; ^u CONICET-National Weather Service, Buenos Aires, Argentina; ^v Space Science and Engineering Center, University of Wisconsin–Madison, Madison, Wisconsin; ^w NorthWest Research Associates, Seattle, Washington; ^x National Center for Marine Environmental Forecasting, Beijing, China; ^y Institute of Polar Sciences (CNR-ISP), Bologna, Italy; ^z Institute for Atmospheric and Climate Science, ETH Zurich, Zurich, Switzerland; ^{aa} Institut des Géosciences de l'Environnement, CNRS/UGA, Saint Martin d'Hères, France; ^{bb} WSL Institut for the Snow and Avalanche Research SLF, Davos, Switzerland

1. Introduction

The Polar Prediction Project (PPP) was a 10-yr (2013–22) initiative of the World Meteorological Organization's (WMO) World Weather Research Programme (WWRP) aimed at significantly improving weather and environmental prediction and services for the polar regions on time scales up to seasons (Jung et al. 2016). Its flagship activity was the Year of Polar Prediction (YOPP). PPP officially concluded at the end of 2022. As part of YOPP, the YOPP in the Southern Hemisphere (YOPP-SH) focused on Antarctica and the Southern Ocean. YOPP-SH started in 2015 and will continue until the end of 2024. A special observing period (SOP) during austral summer was conducted from 16 November 2018 to 15 February 2019, and an overview of the achievements was presented by Bromwich et al. (2020). The 2200 additional radiosondes launched from around Antarctica during the SOP led to marked improvements in weather forecast performance (Bromwich et al. 2022; Choi et al. 2023). The Sea Ice Prediction Network South (SIPN South) demonstrated that the predictability of the sea ice decay around Antarctica during summer had limited skill (Massonnet et al. 2023).

Antarctica poses unique challenges for weather forecasting models. To exemplify this, Fig. 1 contrasts the skill of the European Centre for Medium-Range Weather Forecasts (ECMWF) global deterministic forecast for the Arctic and Antarctic for several lead times. While large-scale extratropical upper-air forecast skill is now almost the same in the Northern Hemisphere and Southern Hemisphere (not shown), the tropospheric predictability skill in Antarctica lags of 8–10 years behind that of the Arctic. The difference originates mainly from relatively low skill along the Antarctic coast during the austral winter (not shown).

As a result, the YOPP-SH community decided that atmospheric predictability during austral winter should also be explored. Part of the motivation was the increasing evidence of rapid climate change impacting Antarctica, signified by the low sea ice coverage since 2016

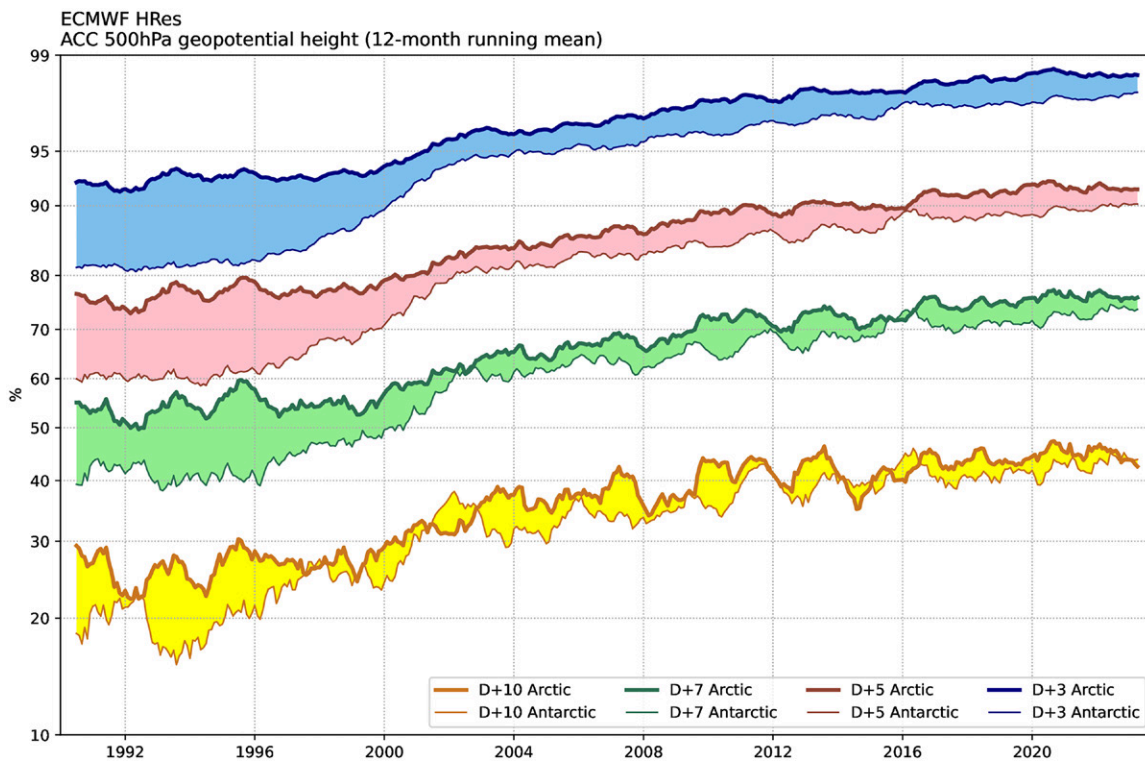


FIG. 1. Evolution of forecast skill at different lead times (days 3, 5, 7, and 10) in the Arctic (thick lines) and Antarctic (thin lines). Shown is the 12-month running mean of anomaly correlation coefficient (ACC; %) of 500-hPa geopotential verified against analysis for the HRES operational run of ECMWF's Integrated Forecasting System (IFS). The difference in forecast skill between the two regions, indicated by the colored areas between the running-mean lines, decreased markedly in the late 1990s coinciding with the start of the satellite microwave radiance assimilation (e.g., Simmons and Hollingsworth 2002) but has remained nearly constant since then. The polar regions are defined here as north of 60°N and south of 60°S.

(Massonnet et al. 2023). An additional motivation was the growing interest in year-round scientific investigations and the associated support needed; one example is winter sea ice studies in McMurdo (McM) Sound close to Scott Base that were conducted by New Zealand colleagues during the SOP. Consequently, a new SOP from 16 April to 31 August 2022 was organized. In view of the limited personnel and physical resources available during the winter, a modified observing strategy from the summer was developed. Under the SOP umbrella, enhanced radiosonde releases and in situ process observations were focused on targeted observing periods (TOPs) of 5–10-day duration each, fashioned after the TOP conducted in the Arctic (Svensson et al. 2023).

This manuscript provides an overview of the winter TOPs conducted during YOPP-SH and summarizes the first results. It is organized as follows. The next section describes the forecasting that was undertaken to decide the start of the seven TOPs along with the forecast tools utilized. Early and impactful tests of the forecast impact of the additional TOP radiosondes are presented. The SOP prominently features atmospheric rivers (ARs), and we provide a synthesis of regional observations of clouds and precipitation from the Antarctic Peninsula, which are instrumental in refining model parameterizations of these processes. In a similar manner, a section focusing on the dynamics and microphysics of an AR impacting Davis Station in coastal East Antarctica is then summarized. Early results from the YOPP Model Intercomparison and Improvement Project (YOPPsiteMIIP) that is intended to test model process representations against detailed station observations are outlined. An evaluation of weather forecast usage by Antarctic tour operators is then presented and followed by a section exploring the predictability of Antarctic sea ice during the growth season. Conclusions round out the manuscript.

2. Austral winter TOPs

The TOPs were focused on the scientific goals of improving numerical weather prediction (NWP) via enhanced radiosonde observations, better characterizing large oceanic cyclones and ARs impacting coastal Antarctica, and testing and enhancing the prediction of clouds and precipitation by weather forecast models. Figure 2 shows the radiosonde sites participating in the winter TOPs. Based on the summer experiment (Bromwich et al. 2022), efforts were made to entrain lower-latitude stations with the aim of improving the forecasting for major events affecting Antarctica from the north. Twenty-four stations participated with observations from 14 national Antarctic programs and Weather Services, namely, Argentina, Australia, Chile, China, France, Germany, Italy, Japan, Korea, New Zealand, Portugal, Ukraine, United Kingdom, and the United States.

To initiate the TOPs, forecasting teams were assembled for two broad regions of Antarctica, namely, the Antarctic Peninsula–Weddell Sea region (including Neumayer Station at 8°W) and East Antarctica spanning Syowa Station at 40°E eastward to the Ross Sea. The forecasting teams' aim was to announce the commencement of a TOP at least 5 days before the target weather system(s) predicted landfall on the Antarctic coast. This allowed the Antarctic observing community at least 2 days to mobilize and plan rosters, before commencing their

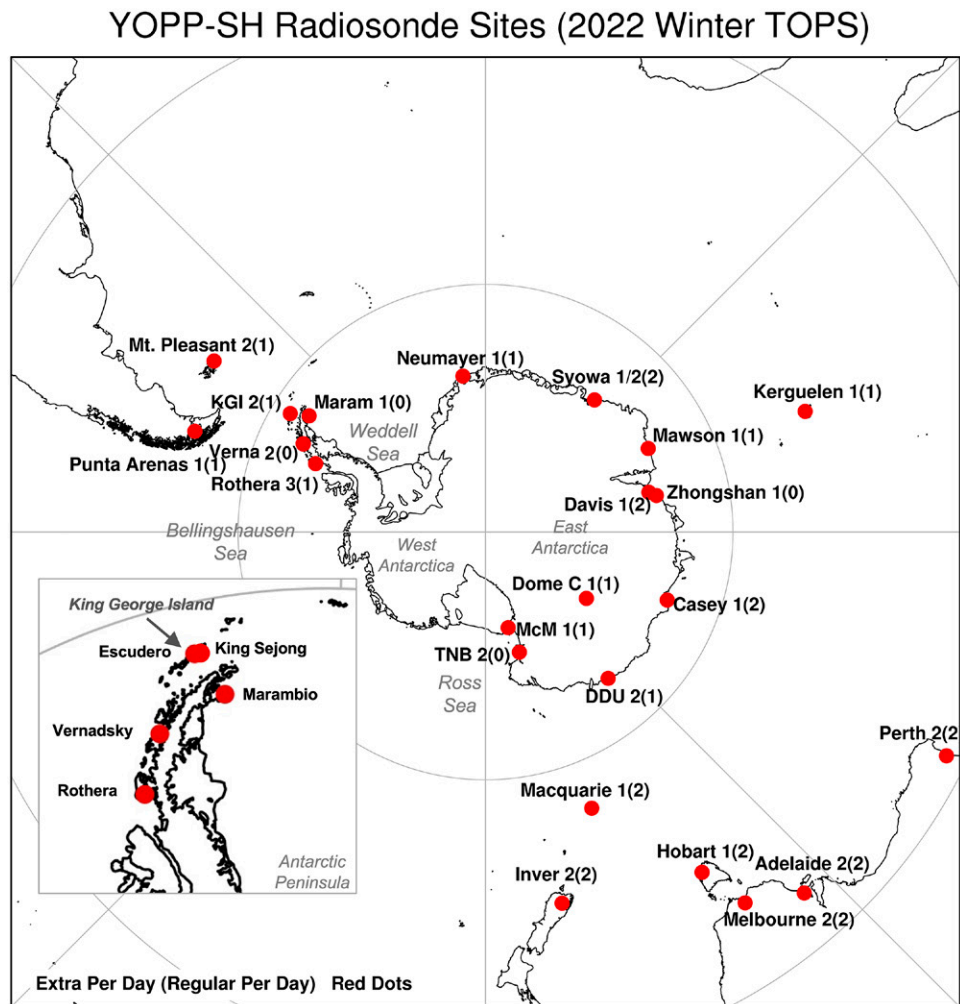


FIG. 2. Stations releasing additional radiosondes during the winter TOPs. The number of additional radiosonde ascents each day is listed for each site next to the site names, and the number of regularly scheduled ascents is enclosed in parentheses. Abbreviated names have been used for Invercargill (Inver), Dumont d'Urville (DDU), Terra Nova Bay (TNB) where two sites are combined, McM, Verna, King George Island (KGI) again with two sites, and Marambio (Maram). The inset zooms up on the AP, and observations from Escudero, King Sejong, and Verna are employed in Fig. 8.

intensive TOP sampling of the environment, spanning antecedent conditions from 3 days prior to landfall to 2 days postlandfall. The challenge of skillfully predicting significant weather 5 days ahead was beyond the comfort range of the more experienced Antarctic forecasters. A shorter forecasting period was adapted for the Antarctic Peninsula–Weddell Sea region, with a heads-up email sent 3 days before the TOP start (6 days prior to event peak/landfall) and advising the stations participating in TOPs of a go decision no later than 48 h before the start of each TOP.

Additional days of dialog were also required before consensus could be reached. This inspired the experimental use of extended-range ensemble products by the Bureau of Meteorology's Australian Community Climate and Earth-System Simulator Seasonal (ACCESS-S) model and the ECMWF, which extended to +3 months and +46 days, respectively. The use of long-range forecasts was novel and had heretofore only been rarely used in Antarctica, on account of their questionable skill in the Antarctic and their limited utility in supporting Antarctic transport and logistical operations. Ultimately, these multiweek outlooks were found to be useful to focus attention on prospective large-scale weather anomalies relative to the climate. The multiweek forecasts facilitated early discussions about the accuracy of the predictions and their effectiveness in achieving the YOPP objectives, ultimately aiding in the strategic planning of the TOPs.

Higher-resolution deterministic and ensemble forecast products from the Antarctic Mesoscale Prediction System [AMPS, using the Weather Research and Forecasting (WRF) Model], the Bureau of Meteorology's ACCESS-Global, National Centers for Environmental Prediction's Global Forecast System (NCEP GFS), Météo-France Action de Recherche Petite Echelle Grande Echelle (ARPEGE), and the ECMWF were consulted more rigorously within the <10-day prediction range. Additionally, the high-resolution ensemble prediction system Agencia Estatal de Meteorología (AEMET)-gamma short-range ensemble prediction system (γ SREPS; Gonzalez et al. 2020), using several nonhydrostatic (convection permitting) model ensembles, was used for kilometer-scale forecasts over the northern Antarctic Peninsula.

A standardized pan-Antarctic outlook was routinely prepared 3 times per week by Arthur Cayette of the Naval Information Warfare Center (NIWC), Atlantic, and Polar Programs management office as a contribution to the study (Fig. 3). The outlook was extended first to +7 days but was then extended to +10 days on request from the YOPP-SH TOP planning team. The process used was first to review the steering patterns from the 400–200-hPa levels. The 300-hPa level was displayed in the outlook summaries due to ready availability from AMPS, NCEP GFS, and ECMWF. Midlevels of 850–500 hPa were considered to help determine the depth and intensity of shortwave systems. The YOPP team sought scenarios where large-scale moisture pulses, sometimes staggered, of near-full tropospheric depth were being steered into the continent by cohesive upper-level, meridionally oriented jets. Ultimately, large-scale forcing of this type is required to overcome the blocking effects of cold air damming and steep terrain, which will otherwise significantly delay or minimize the impacts of moist intrusions into the continent's interior. Too-coarse resolution of the topography or improper depictions of the intensity or location of cloud masses, jet streams, temperature gradients, or pressure gradients by numerical models can produce false moisture transport into the continent's interior. Remote automatic weather station (AWS) data and satellite observations were the primary sources for confirmation of, or bias adjustments to, the forecasts. The Antarctic Meteorological Research and Data Center (AMRDC) collected and made available these observational datasets.

To better identify and quantify the impact of ARs on Antarctica during the TOPs, the Center for Western Weather and Water Extremes (CW3E) at the Scripps Institution of Oceanography developed an AR scale specific to the polar regions, which have a colder, drier, and more pristine environment (Zhang et al. 2024, manuscript submitted to *Cryosphere*). The polar AR scale includes rankings of AR-P1, AR-P2, and AR-P3 in addition to the Ralph et al. (2019) AR1 through

Discussion



Issued Thursday July 21, 2022 for the next 5 days until Tuesday July 26, 2022. (Based on 300 hPa and AR predictions from AMPS that are not shown because of space limitations)

Upper-level circulation

There are two primary northerly flows (at 300 hPa) onto the Antarctic continent, one centered over Wilkes Land and the other over the Antarctic Peninsula. A northerly jet flow over Casey Station will continue during the period. The flow over the Antarctic Peninsula will be pushed north as the upper low repositions; this will drive the jet max. around the Peninsula into the Weddell Sea by Monday July 25. The flow will stay strong over the northern tip of the Peninsula through Tuesday July 26.

Low-level circulation highlights

- A low-level cyclone stalling just offshore from Casey Station will move an AR over Wilkes Land that will migrate eastward over George V Land early next week.
- Current low on the Ross Ice Shelf will move east of Ross Island. The remainder of the period will be dominated by flow from interior Antarctica.
- Migratory lows transiting through the Bellingshausen Sea will provide the most activity and are linked with fast moving ARs that move into the Weddell Sea over the weekend.

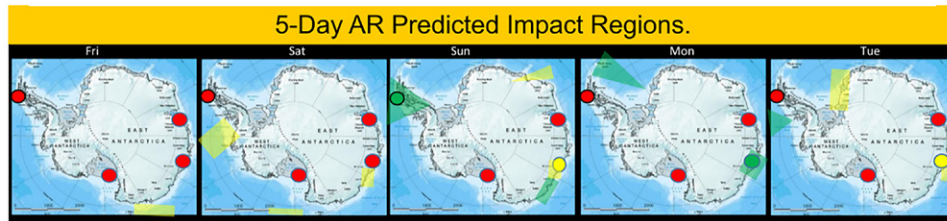


FIG. 3. Simplified example of 10-day forecast outlook prepared by Arthur Cayette, NIWC, Atlantic, Polar Programs IPT focusing on Davis, Casey, McM, and Palmer stations and the prospect of ARs in their vicinities. (bottom) Colors correspond to the TOP recommendations in the headlight display at the top. Because of space limitations, only material for the first five forecast days is shown. These outlooks were produced 3 times a week during the entire SOP by Arthur Cayette.

AR5 rankings as shown in Fig. 4d for the northern tip of the Antarctic Peninsula (Zhang et al. 2024, manuscript submitted to *Cryosphere*). The scale is determined based on the duration of AR conditions [integrated water vapor transport (IVT) magnitude $> 100 \text{ kg m}^{-1} \text{ s}^{-1}$] and the maximum IVT magnitude during an AR at a specific location. The minimum IVT magnitude threshold of $100 \text{ kg m}^{-1} \text{ s}^{-1}$ is utilized instead of $250 \text{ kg m}^{-1} \text{ s}^{-1}$ for the regular AR scale (Ralph et al. 2019) due to lower specific humidities in the polar environment. The CW3E polar AR scale forecast tool (https://cw3e.ucsd.edu/arscale_antarctica/) provided real-time information of AR intensity and duration along the Antarctic coastline and at targeted weather stations based on NCEP Global Ensemble Forecast System (GEFS) forecasts. Figure 4 shows an example of a CW3E polar AR scale forecast for Antarctica on 10 May 2022. During the YOPP-SH winter TOPs, the CW3E polar AR scale forecast tool was used in forecast operations in addition to other forecast products to guide radiosonde launches for the TOPs. The CW3E polar AR scale also supported research on extreme weather events triggered by ARs in polar regions, such as heatwaves, surface melting, and heavy precipitation (e.g., Wille et al. 2024a,b; Zou et al. 2023; Gorodetskaya et al. 2023).

Specifically, for the Antarctic Peninsula–Weddell Sea forecasts, the ECMWF products were organized in a dedicated dashboard, including extended-range forecasts (up to 1 month) of mean sea level pressure (MSLP), 2-m temperature, and precipitation (with upper 10th percentile) over Antarctica and Southern Ocean, as well as for the stations participating in the winter TOPs (Fig. 5). Further, the high-resolution (HRES) deterministic forecast (9-km resolution, 137 levels, to 10 days ahead) and the ensemble (ENS) forecasts (51 members, 18-km resolution,

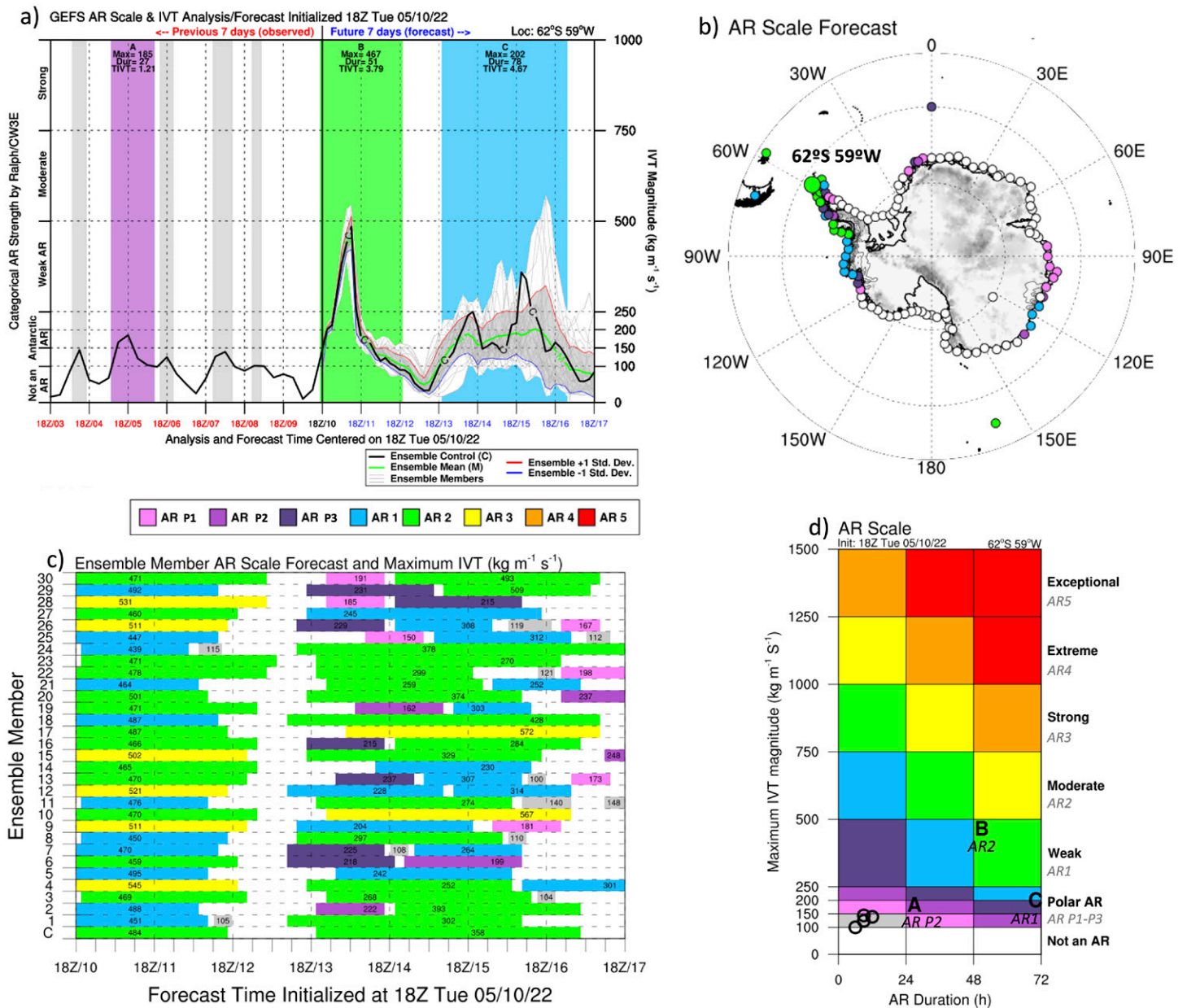
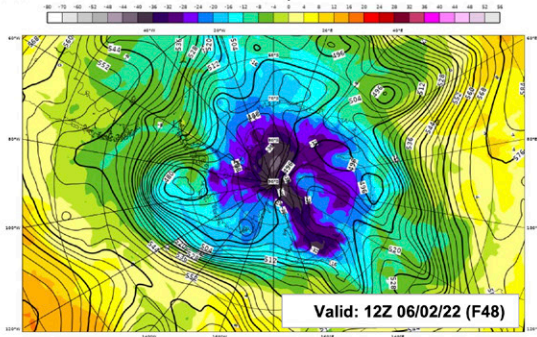


FIG. 4. Example of CW3E polar AR toolkit on 10 May 2022 at the northern AP. (a) The plume diagram represents the IVT forecast for each of the NCEP GEFS ENS members (thin gray lines), the unperturbed GEFS control forecast (black line), the ENS mean (green line), and plus or minus one standard deviation from the ENS mean [red line (+), blue line (-), and gray shading]. Colored shading represents the AR scale forecast for the given time, calculated using the model control forecast. (b) Dots on the map represent the maximum AR scale forecast from the GEFS control member at that grid point for the next 7 days. The enlarged dot indicates the location for (c) AR forecasts. (c) AR scale magnitude and timing calculated for each GEFS ENS member shaded according to scale. Values within the shading represent the magnitude and timing of maximum IVT during each forecasted AR at 62°S, 59°W. Gray shading in each panel represents IVT > 100 ($\text{kg m}^{-1} \text{s}^{-1}$) for a duration <24 h. (d) Letters represent where each AR identified by (a) (color shaded regions) fall on the polar AR scale matrix and how the AR scale is calculated for each. Circles correspond to vertical gray shadings in (a) where IVT exceeds 100 ($\text{kg m}^{-1} \text{s}^{-1}$) for <24 h.

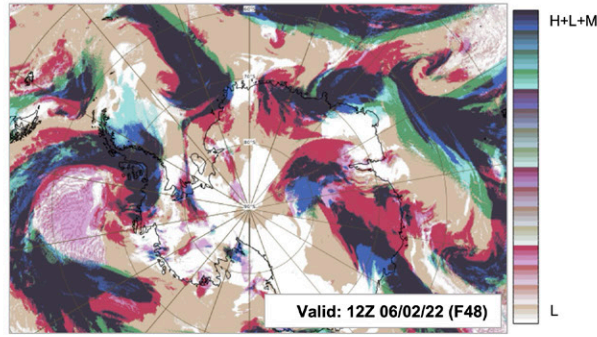
137 levels, to 15 days ahead) were utilized. HRES forecasts were used to examine the charts of 2-m temperature with 30-m winds, geopotential at 500 hPa with temperature at 850 hPa, precipitation and MSLP, precipitation type, total cloud cover, and total column water vapor. For each station participating in the TOPs, HRES forecasts of the vertical profiles (using tephigrams) and wind hodographs were consulted. HRES forecast and ENS distribution were combined in the 10-day meteograms for each station showing 2-m temperature, 10-m wind speed and gust, total cloud cover, total precipitation and snowfall, and probability of precipitation type in precipitation rate categories (rain, sleet, wet snow, snow, ice pellets, and freezing

ECMWF HRES forecast

500hPa GeoP and 850hPa Temp

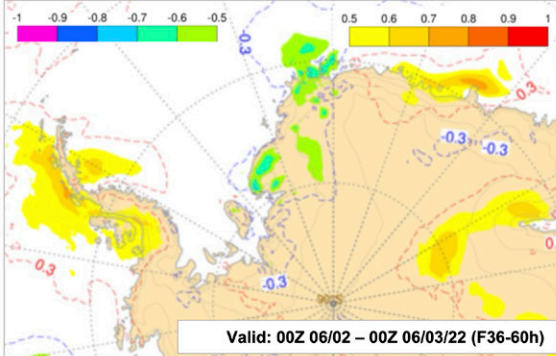


Total Cloud Cover

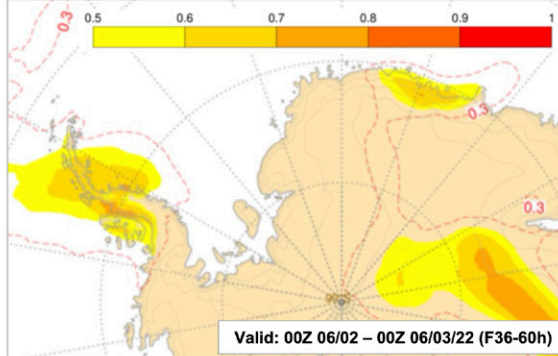


ECMWF Extreme Forecast Index for 2-m temperature and water vapor flux

Extreme Forecast Index (EFI) 2m maximum temperature



Extreme Forecast Index (EFI) water vapor flux



Meteogram of Total Precipitation, 2-m Temperature and precipitation type (Escudero)

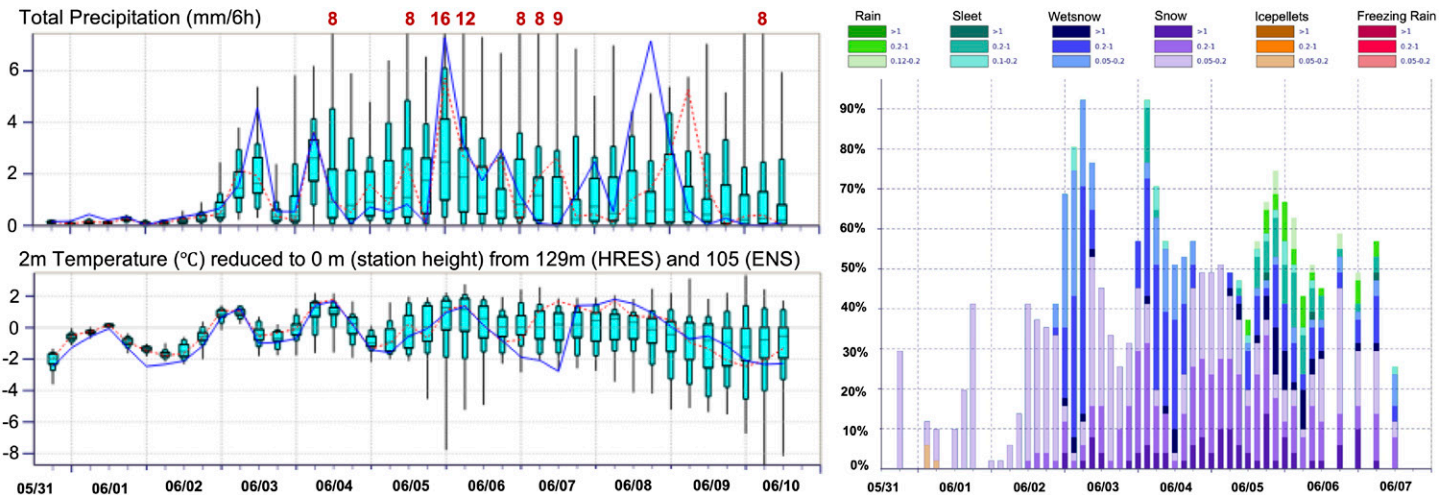


FIG. 5. Simplified example of the 10-day outlook provided every 3 days by the AP–Weddell Sea region forecasting team for 2–3 Jun 2022: 500-hPa geopotential (4 dam contour interval) with 850-hPa temperature (4°C contour interval, spanning $\sim -36^{\circ}\text{C}$ over Antarctica in black to $+14^{\circ}\text{C}$ in lower left in orange) and total cloud cover (from low to high + low + medium level cloud cover) from the ECMWF HRES forecast; ECMWF EFI for 2-m temperature and IVT; and ECMWF ENS meteograms for total precipitation and 2-m temperature for Escudero. The solid blue line shows the evolution of the HRES forecast. Boxplots represent (from bottom to top) minimum, 10th percentile, 25th percentile, median, 75th percentile, 90th percentile, and maximum. (top) Precipitation maxima extending beyond the plot range are given in red numbers; ECMWF ENS precipitation type meteogram for Escudero specifying the probability of precipitation type (%) in precipitation rate categories (mm h^{-1}) [(from bottom to top) 0.1–0.2, 0.2–1, and >1].

rain); see Fig. 5. Finally, the extreme forecast index (EFI) product pioneered at ECMWF was used, which is a measure of the difference between the ensemble forecast distribution and a model climate distribution. Complemented by the shift of tails (SOT), EFI is considered an “alarm bell” for extreme weather situations (e.g., Zsoter 2006). In the TOP decision-making, EFI for wind speed, 2-m maximum temperature, water vapor flux, and precipitation were used.

Targeted Observing Periods (TOPs)



FIG. 6. YOPP-SH winter TOPs conducted. Photographs clockwise from the top right show TOP radioonde releases from McM, Neumayer, Kerguelen, and Syowa stations with the Aurora Australis in the background at Syowa.

Another experimental model for the Antarctic Peninsula tested during the YOPP-SH winter campaign was the AEMET- γ SREPS mentioned previously. Although this model was not useful for the 5-day forecasts required for announcing the TOPs, it gave interesting detail of the short-term uncertainty associated with each event. For the events of smaller magnitude, the spread can be too large, and the event development time can be shortened by 1–2 days to use a more reliable forecast (<5 days), keeping the same station TOP alerting schedule.

Based on the abovementioned tools and discussions, seven TOPs were conducted during the SOP. Figure 6 provides an overview of them. Four involved both the Antarctic Peninsula and East Antarctica, so-called pan-Antarctic or circum-Antarctica, that are most effective for improving NWP in the Southern Ocean and Antarctica. Two solely considered East Antarctica, and one considered the Antarctic Peninsula. The Antarctic Peninsula TOP5 immediately preceded the second East Antarctic TOP6, so together they form a fifth pan-Antarctic TOP. A total of ~1100 additional radiosonde ascents were launched, more than doubling the routine number of soundings at the stations shown in Fig. 2.

High-time-resolution radiosonde data during the TOPs were collected from around 60 radiosonde stations and two ships in the Antarctic, sub-Antarctic, and surrounding landmasses (details not shown). High-time-resolution radiosonde data have frequent data reporting (e.g., every 2 or 3 s of flight), while traditional radiosonde data have fewer levels reporting only at mandatory levels (e.g., 1000, 925, 850, and 700 hPa) and significant levels (where there are significant changes in temperature, moisture, or wind to report). The data were primarily collected at National Center for Atmospheric Research (NCAR) from the Global Telecommunication System (GTS) after being transmitted in Binary Universal Form for Representation of Meteorological Data (BUFR) format. Data that did not get on the GTS from the stations shown in Fig. 2 were collected from the station operators to make the dataset as complete as possible. Archival of these observations together with the polar AR data discussed above is at the Antarctic Meteorological Research and Data Center (<https://amrdcdata.ssec.wisc.edu/group/year-of-polar-prediction-in-the-southern-hemisphere>).

3. Data impact modeling studies

A study of The Ohio State University (OSU) and NCAR is investigating the impact of the YOPP-SH TOP special radiosonde data on NWP model forecasts using the AMPS infrastructure. The study applies AMPS' WRF Model (Skamarock et al. 2019) in experiments involving the assimilation of the soundings to evaluate their impact on TOP forecasts of the campaign's weather foci (i.e., ARs and cyclones). The WRF domain setup for the study has two model grids with

horizontal grid spacings of 24 km (outer frame, similar domain as shown in Fig. 2) and 8 km, spanning Antarctica out to $\sim 60^{\circ}\text{S}$ (not shown).

The main model experiments vary the observations assimilated using either the multiresolution incremental four-dimensional variational data assimilation (MRI-4DVAR) technique (Liu et al. 2020) or the three-dimensional ensemble variational data assimilation (3DEnVar) (Wang et al. 2008) approach. In this investigation, 5-day WRF forecasts are begun at 0000 and 1200 UTC for each day of each TOP, with all seven winter TOPs being simulated. There are two forecasts for each starting time: one based on a model initialization assimilating only the routine atmospheric observations¹ and one from an initialization in which the TOP special soundings are added to the set of routine observations. Thus, these experiments aim to reveal the effects of the extra TOP soundings on Antarctic forecasts.

As an example of some of this work, cycling assimilation with 3DEnVar was performed in 6-h increments starting 2.5 days before the commencement of TOP3 (East Antarctica) from the GFS initial conditions and continued through the TOP duration. Figure 7 shows the impact of the extra assimilated radiosonde observations on the forecast of a synoptic-scale

¹ The routine observations used here are as follows: surface data [e.g., AWS, surface synoptic observations (SYNOP), and METAR]; upper-air soundings; aircraft observations; ship and buoy observations; geostationary and polar-orbiting satellite atmospheric motion vectors (AMVs); GPS radio occultations; and satellite radiances.

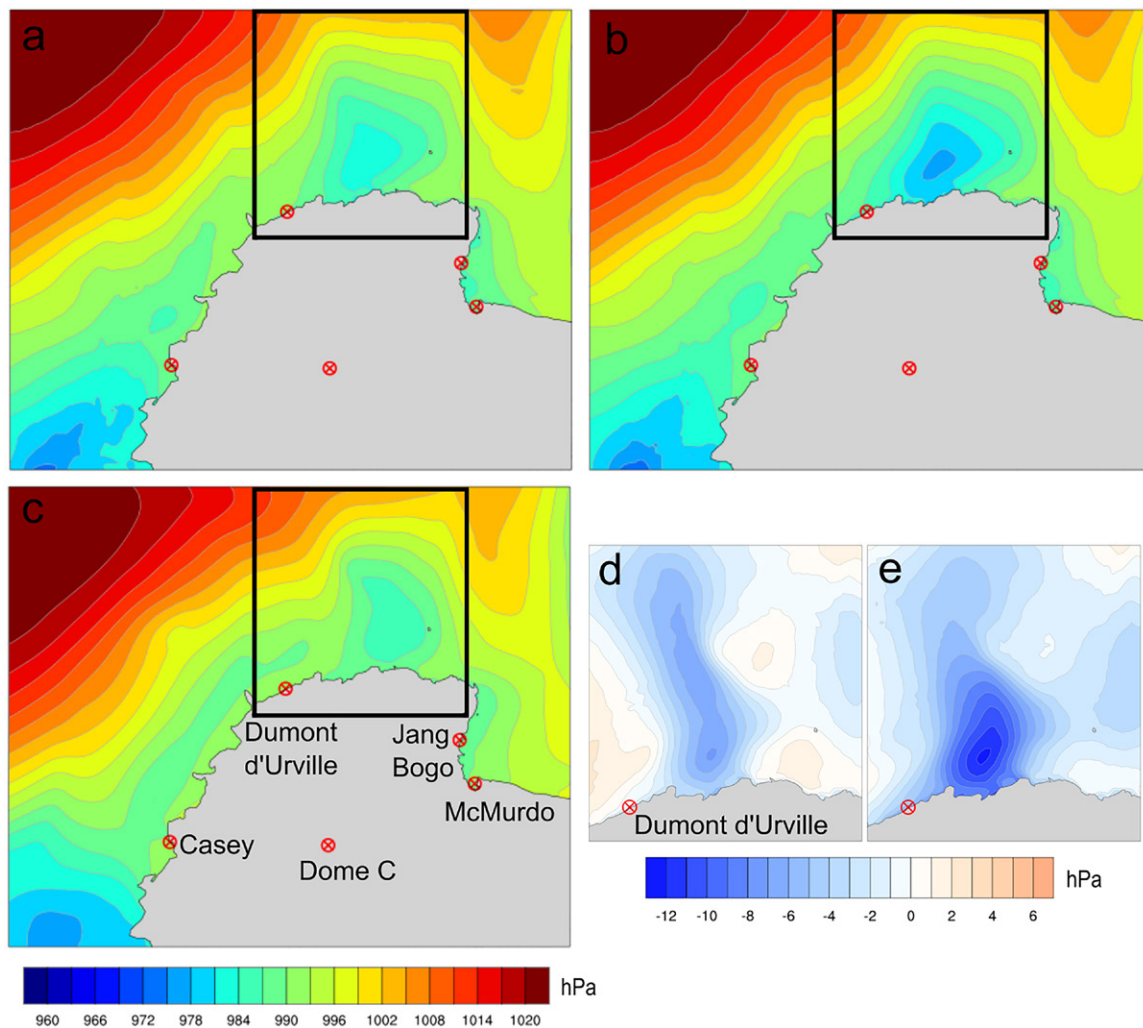


FIG. 7. MSLP at 1200 UTC 7 Jul 2022 during TOP3. (a) 60-h TOP forecast assimilating extra radiosondes; (b) 60-h TOP forecast without extra radiosondes; and (c) ERA5 global reanalysis. (d) Bias of forecast (a) in relation to ERA5 adjacent to DDU Station. (e) Bias of forecast (b) in relation to ERA5. Forecast initial time is 0000 UTC 5 Jul 2022. Sites releasing extra radiosondes during TOP3 are shown by red circles with a cross and are labeled in (c). Zoomed region for (d) and (e) shown in (a)–(c). Contour interval is 3 hPa in (a)–(c) and 1 hPa in (d) and (e).

cyclone to the east of Dumont d'Urville Station. This region, off the Adelie Land coast, is among the most active cyclogenesis regions in the Southern Hemisphere (Hoskins and Hodges 2005; Bromwich et al. 2011), and typically, cyclones develop there or intensify in low-pressure troughs that extend eastward from intense coastal lows. We employ the ERA5 global reanalysis as a benchmark for evaluating the forecasts. The fidelity of ERA5 was confirmed for TOP3 by comparing radiosonde observations of temperature, wind speed, relative humidity, and geopotential height at five levels with ERA5 values for each of the five stations shown in Fig. 7; biases for all variables for the ~20 soundings at each station were small, and correlation coefficients mostly exceeded 0.95. The assimilation of only routine soundings substantially overdevelops the low east of Dumont D'Urville (Fig. 7b) in comparison with the ERA5 reanalysis (Fig. 7e; by up to 13 hPa). While the addition of the TOP special soundings still results in an overly deep cyclone in the 60-h forecast (viz., by up to 6 hPa; Fig. 7a), the simulated low is much closer in intensity and structure to that in the ERA5 reanalysis than the forecast using only the routine soundings (Figs. 7d,e). The prior work of Chen et al. (2014) suggests that forecast models tend to overintensify such Adelie Coast cyclones, where limited observations for initialization are present. That study tested the forecast impact of assimilating GPS radio occultation observations and found that their addition mitigated the overintensification of a similar cyclone via a reduction in simulated baroclinicity. These cyclones track to the east and south and can bring poor weather to McMurdo Station (Bromwich et al. 2011), impacting operations. Ongoing research is studying all of the TOPs to determine the benefits from the additional radiosonde launches on forecasts of major cyclones and ARs affecting coastal Antarctica and the reasons for them.

4. Antarctic Peninsula: Clouds and precipitation observations during an atmospheric river event

The Antarctic Peninsula (AP) is a narrow, glaciated mountain ridge making up part of West Antarctica and is characterized on its western side by much milder climate compared to the rest of the Antarctic continent. The AP is highly sensitive to the impacts of ARs, which can bring both intense snowfall and major surface melt events affecting the stability of its ice shelves and playing an important role in the AP surface mass balance (Wille et al. 2019, 2021, 2022; Gorodetskaya et al. 2023; Zou et al. 2023). Thus, ARs have been a major focus of the winter TOPs. Five stations located in the AP participated in the winter TOPs, contributing enhanced observations representing different regional meteorological regimes and impacts (Fig. 2). Here, we describe physical processes associated with an AR event during TOP1 using observations from three sites: Vernadsky (Verna), located in the northwestern AP; and two stations on King George Island (KGI) (located 10 km apart)—King Sejong and Escudero. In addition to radiosonde releases, each site measures standard long-term near-surface meteorological variables, broadband radiative fluxes, visibility, and precipitation. Vernadsky and Escudero stations each had precipitation profiling with a Micro Rain Radar (MRR-PRO and MRR-2 models, respectively). These are 24-GHz vertically profiling radars for Doppler spectra of hydrometeors, from which snowfall and rainfall properties were derived using the Ferrone et al. (2022) algorithm for snow and the Peters et al. (2010) methodology for rain. Lidar cloud profiling with mini-micropulse lidar (MPL) measurements was available at Escudero as part of the MPLnet network (Lewis et al. 2016).

During TOP1, three short AR episodes affected the AP. The third AR, originating from the Pacific, is discussed here and affected the AP from 0000 to 0900 UTC 16 May (Fig. 8a). Figure 4 shows that 6 days before an AR1 was forecast to be in the vicinity, illustrating that the forecast guidance was very useful in preparing for the acquisition of enhanced observations.

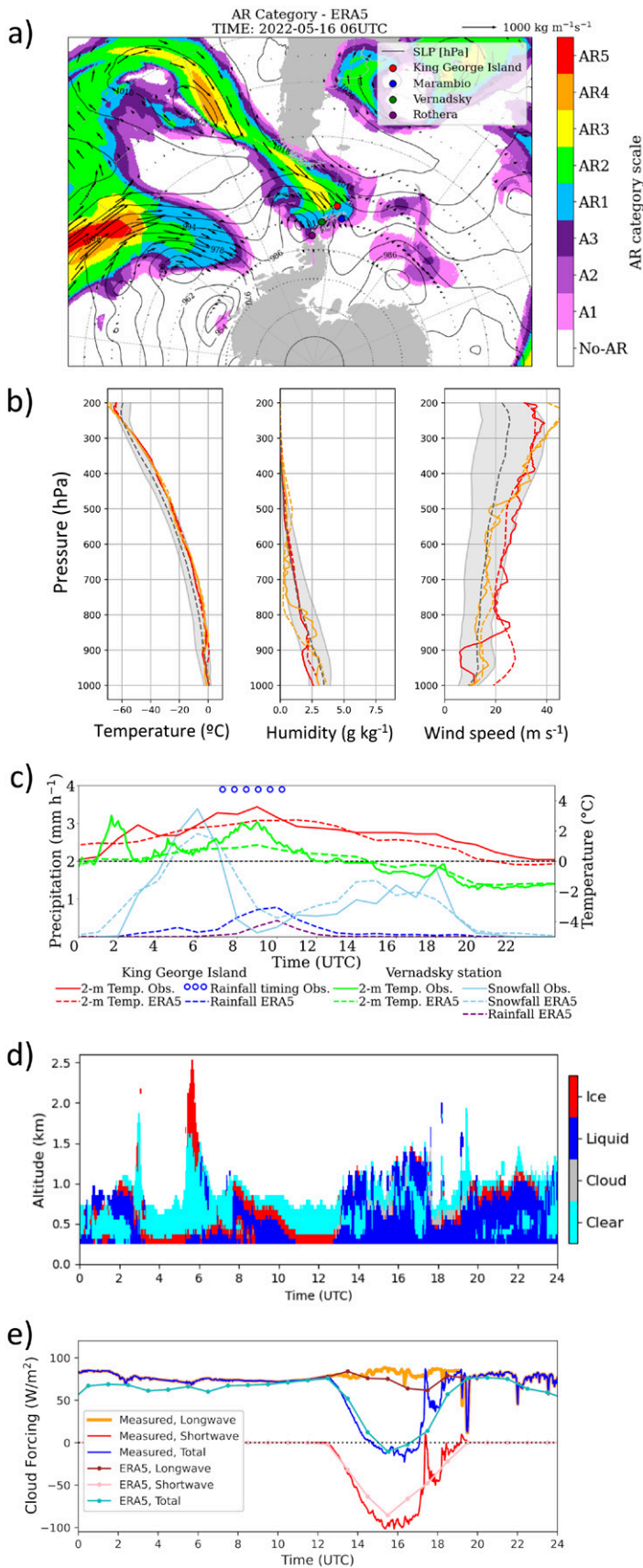


FIG. 8. AR and its impacts at the AP during TOP 1: (a) CW3E AR scale for the AR impacting the northern AP on 16 May 2022. (b) Radiosonde profiles of temperature, specific humidity, and wind speed at KGI: Solid-colored lines show radiosonde observations for the two launches when the last AR during TOP1 was making landfall—on 0000 UTC 16 May (orange) and 1200 UTC 17 May (red); dashed colored lines show ERA5 profiles at the nearest grid points at respective times; ERA5 climatological profiles for May 2012–22: black dashed = median and gray shading = two standard deviations. (c) 2-m temperature and precipitation data from ERA5 and observations at KGI and Verna Station. The 2-m temperature observations are sourced from the AWS at King Sejong and Verna. Rainfall observations at KGI are derived from MRR-2, indicating occurrences $>0.1 \text{ mm h}^{-1}$. Verna snowfall observations are based on snowfall rate S estimates using MRR-PRO equivalent radar reflectivity factor Z_e and the Kulie and Bennartz (2009) methodology for aggregate snowflakes (most relevant to the observed snowfall event properties). The horizontal black dashed line emphasizes the 0°C limit. Time is UTC hours on 16 May. (d) Cloud mask from the MPL showing phase and vertical extent derived using methodology by Stillwell et al. (2018). (e) Measured and ERA5 downward cloud forcing at the surface, defined as the (cloudy) downwelling radiation minus the simulated clear sky downwelling radiation, for longwave, shortwave, and total (longwave + shortwave) at Escudero (KGI) on 16 May 2022. Positive numbers indicate positive downward forcing at the surface.

Each of these AR episodes was marked by an increase in 2-m air temperature above 0°C at all AP stations participating in TOPs (see Fig. 8c for King George Island and Vernadsky on 16 May). Radiosonde profiles show that during the AR landfall on the AP (15–17 May), temperatures at King George Island were the highest compared to the 10-yr range throughout

the troposphere and the lowest at the tropopause (Fig. 8b). Specific humidity and wind speed reached a maximum between 800 and 900 hPa driving the highest moisture transport within this layer (Fig. 8b). ERA5 reanalysis represents well the thermodynamic structure in the upper troposphere, but with significant discrepancies compared to observations below 700 hPa (particularly for wind speed and humidity and to a smaller extent for temperatures). The lower-troposphere thermodynamic structure is important for clouds and precipitation, impacting their microphysical properties.

Rainfall was observed on King George Island (northern AP) during two distinct periods, with ERA5 effectively capturing the timing of the first moderate-intensity rainfall, corroborated by ground-based radar measurements at Escudero (Fig. 8c) and 3.6 mm of rainfall measured at the adjacent Frei Station between 0600 and 1200 UTC. At the same time, Vernadsky Station (situated in the northwestern AP) predominantly experienced snowfall during the AR event according to observations, despite near-surface temperatures reaching 2°C. Unlike observations, ERA5 also showed a small amount of rain at Vernadsky. Radar profiles from Vernadsky revealed the event's initiation with virga (not shown) and intensifying snowfall at the surface (Fig. 8c). A high radar reflectivity band and temperatures above 0°C suggested the melting layer was near the surface during AR landfall. Snowfall diminished in intensity during the second part of the event, with sublimation reaching approximately 25%. Precipitation rates from both radar and ERA5 at Vernadsky exhibited good agreement in timing, variability, and precipitation phase. Overall, the findings highlight the complex nature of precipitation formation and evolution during an AR event, particularly snowfall–rainfall transitions in terms of temporal and spatial variability. This also emphasizes the imperative to enhance quantitative precipitation estimation in the AP.

Clouds have a strong influence on the Antarctic surface energy budget through both cooling and warming effects that depend on cloud thickness, height, and phase. Cloud phase is particularly important since liquid clouds typically trap more infrared radiation than ice clouds. MPL measurements at Escudero were used to produce a cloud-phase mask showing the presence of near-surface liquid clouds over most of the day (Fig. 8d; note that ice at the top of liquid cloud is most likely liquid that has been misidentified due to multiple scattering off the cloud top). Extended periods of weak rainfall after 0600 UTC were indicated by the precipitation radar (Fig. 8c). For most of the day, the vertical cloud extent observed by the MPL was limited to 1–1.2 km above ground level (below 850–900 hPa) (Fig. 8d), the layer within which the AR had its core with temperature maxima slightly exceeding 0°C (Fig. 8b). These low-level clouds with warm cloud-base temperatures (Figs. 8b,d) led to relatively high downwelling longwave fluxes throughout the day (up to 325 W m⁻²; not shown) and were consistent with downwelling longwave cloud forcing of around 70–90 W m⁻² all day (Fig. 8e). Due to the time of year, shortwave radiation was low. Furthermore, the cloud was thick enough to block much of the shortwave radiation, with only about 20% making it through the cloud, leading to a shortwave cloud forcing during the daytime (~1200–1900 UTC), reaching about –100 W m⁻² at solar noon. ERA5 downwelling fluxes agreed fairly well with the measurements. Upward components, needed to calculate the net forcing, were not measured; however, compared to the total downward forcing shown in Fig. 8e, the net forcing is expected to be similar during the nighttime (since the net longwave cloud forcing is expected to be within a few W m⁻² of the downward longwave cloud forcing) and larger during the daytime (since the net shortwave cloud forcing is expected to have a smaller magnitude than the downwelling shortwave forcing, with the reduction depending on the surface albedo). Overall, therefore, the net cloud forcing was strongly positive during the nighttime and likely slightly positive during the day, indicating that the clouds had an overall warming effect, as was found to be the case for ERA5.

5. Davis Station: Dynamics and precipitation during an atmospheric river

Davis is located in coastal East Antarctica (Fig. 2) and is sheltered from the prevailing winds by the ice-free Vestfold Hills. Northeasterly winds from the passage of transient extratropical cyclones interact with and enhance the katabatic flow, which create adiabatic winds (foehn) due to the presence of an ice ridgeline upwind of Davis. These warm foehns result in substantial precipitation sublimation in the lowest kilometer of the atmosphere in both summer and winter (Gehring et al. 2022; Alexander et al. 2023). A suite of sensors was deployed to Davis for YOPP-SH, including a Vaisala CT25K ceilometer, an MRR-PRO, and broadband radiometers. These instruments complemented radiosonde launches and a permanently installed very high frequency (VHF) wind-profiling radar, which provides profiles of the horizontal and vertical wind fields (Alexander et al. 2017). Ceilometer data from the Vaisala CT25K are calibrated using periods of opaque stratocumulus clouds (O'Connor et al. 2004) and then processed with a previously trained machine learning algorithm (G22-Davis) as described in Guyot et al. (2022) to estimate the cloud phase using only the calibrated attenuated backscatter. The raw MRR-PRO data are postprocessed following Ferrone et al. (2022), which increases the signal-to-noise ratio and removes instrumental interference lines. The ceilometer records the amount of laser signal scattered by the cloud back to the ceilometer (i.e., the backscatter) at each altitude. Once calibrated (O'Connor et al. 2004), this is referred to as the calibrated backscatter. Similarly, the MRR-PRO records the amount of reflection from precipitating particles at each altitude, and this is referred to as the equivalent radar reflectivity factor or reflectivity for brevity.

An AR, connected to an extratropical cyclone, passed over the region on 3–4 June 2022. The synoptic situation is shown in Fig. 9a at 0349 UTC 3 June, with the extratropical cyclone and associated cloud bands clearly visible. The VHF radar's horizontal wind field captures the event as seen from Davis (Fig. 9b). On 3 June, the midtropospheric winds change from westerly to easterly, although winds at the lowest altitudes sampled by the radar remain easterly but strengthen during the event. Increased vertical wind motion is evident in the latter half of 3 June, which is likely due to orographic wave generation (Alexander et al. 2017; Gehring et al. 2022). Horizontal wind speeds weakened and shifted northerly on 4 June and indications of orographic wave motion ceased at this time.

Above Davis at the time of the satellite image (Fig. 9a), an opaque, low-level mixed-phase cloud is identified (Fig. 9c), with glaciation present between 0400 and 0500 UTC 3 June (Guyot et al. 2022). Later, during the case study, a layer of supercooled liquid, embedded within an ice cloud, is intermittently detected from 1400 UTC 3 June onward (Fig. 9c). This time corresponds to the onset of strong orographic wave activity (see the vertical motion in Fig. 9b) and the presence of warm foehn winds and low relative humidity within the boundary layer (Gehring et al. 2022; Alexander et al. 2023), as indicated by radiosonde data (not shown). This mixed-phase cloud precipitated ice, which is visible as the relatively large amount of signal reflected back to the MRR-PRO (Fig. 9d). As evidenced by the absence of detectable near-surface MRR-PRO reflectivity signal, the ice all sublimated before reaching the ground. Note that reflectivity signal is present in the MRR-PRO data to higher altitudes than the ceilometer's laser backscatter signal, due to the attenuation of the ceilometer's laser beam as it propagates deeper into the optically thick cloud layer. On 4 June, once the foehn winds ceased, intermittent, shallow snowfall was observed by the MRR-PRO near the surface as small increases in the reflectivity. A low-level optically thick ice cloud was present in the ceilometer data at this time. The structure and evolution of this winter event, including the presence of low-level mixed-phase clouds, sublimation, surface snowfall, and liquid water layers within complex, deep mixed-phase clouds, are consistent with summertime observations of cloud systems in this region (Alexander et al. 2021; Gehring et al. 2022).

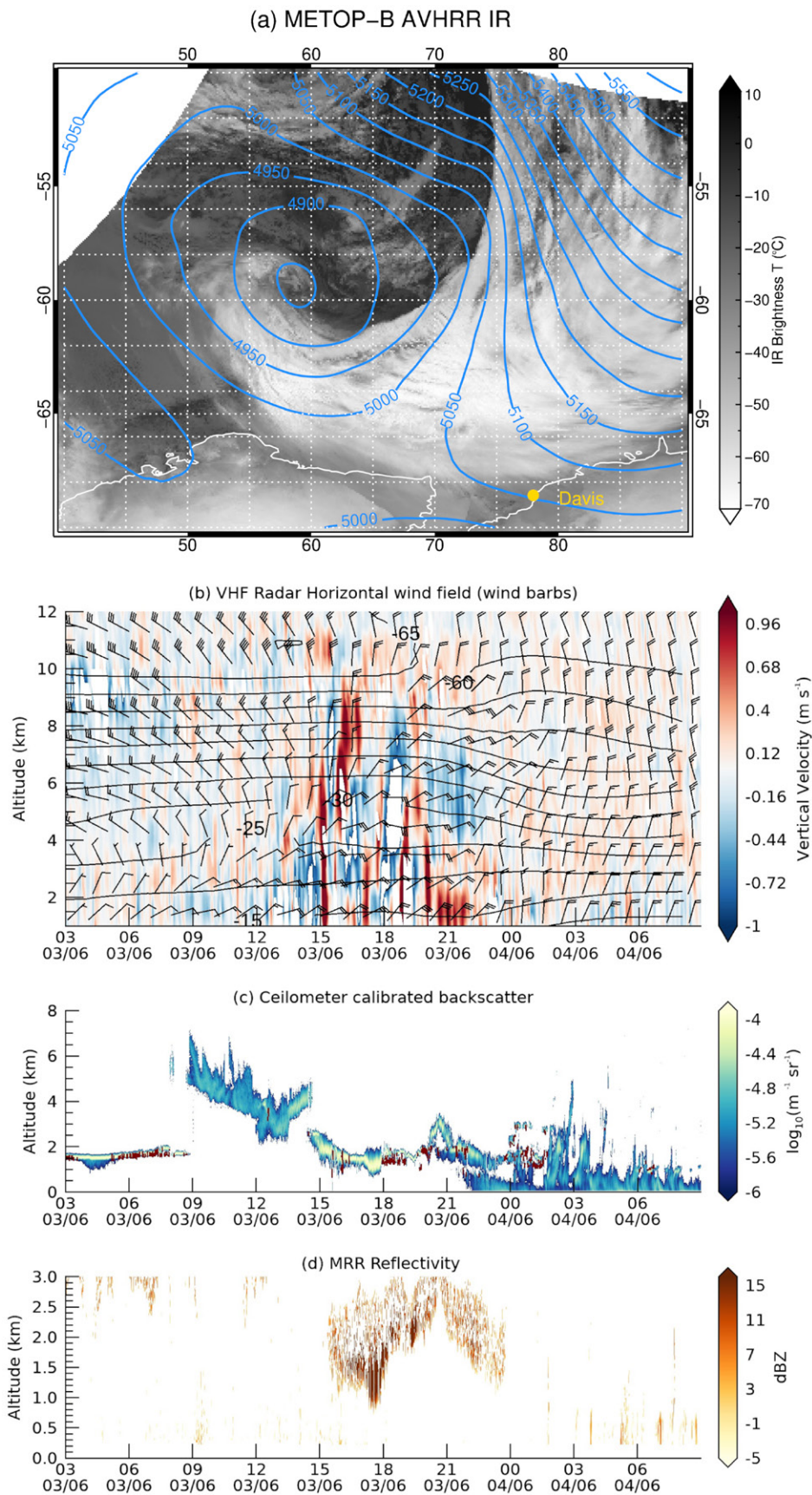


FIG. 9. (a) *MetOp-B* AVHRR IR brightness temperature image at 0349 UTC 3 Jun 2022. ERA5 geopotential heights (m) at 500 hPa are indicated in blue. Davis Station is shown as the yellow circle. The remaining three panels show selected observations made above Davis during 0300 UTC 3 Jun–0800 UTC 4 Jun 2022. Note the varying altitude scales, indicative of the altitude range over which the instruments operate; (b) VHF wind-profiling radar horizontal wind field (wind barbs), vertical wind motion (color scale, upward positive), and ERA5 air temperature field (gray lines, interval 5°C); (c) CTK25 ceilometer calibrated attenuated backscatter (color), with the presence of supercooled liquid water highlighted (red); and (d) MRR-PRO calibrated reflectivity (color; dBZ).

6. Antarctic YOPPsiteMIIP

As part of the WWRP Polar Prediction Project, MIIPs have been running at selected Arctic and Antarctic supersites with collocated process-oriented multivariate observations contributing to the YOPP efforts of intercomparing and improving numerical prediction systems in polar regions (YOPPsiteMIIPs). During YOPPsiteMIIPs, unique datasets for process understanding have been gathered at observatories in both polar regions and effort has been made to make the data more accessible for model evaluation to benefit weather and climate model developments.

One of the goals of YOPPsiteMIIP is to produce the so-called Merged Observatory Data Files (MODFs), which organize multiple variables produced from measurements of various instruments and sources (researchers, institutions, archives, and portals) into a consistent format, which can be used for model evaluation. At the same time, modeling groups participating in the YOPPsiteMIIPs provide the Merged Model Data Files (MMDFs) using consistent naming and metadata, facilitating comparison between models and observations.

In Antarctica, a number of stations have been selected to join the YOPPsiteMIIP effort (Fig. 10a), based on their extensive observational suite or geographic significance. Some of the main physical processes within the focus of the YOPPsiteMIIPs include stably stratified boundary layers, mixed-phase clouds, and interaction with the snow and ice-covered surface and ocean below, as well as air mass transformations during warm air intrusions and cold air outbreaks. Most of these processes were considered when calling the TOPs during the winter YOPP-SH SOP.

Several models have contributed to the winter YOPP-SH period with enhanced and dedicated forecasts (see earlier section on Austral winter TOPs). The Météo-France Research Center provided three different products on a daily basis: 1) a 10-day forecast based on the operational global model ARPEGE used for numerical weather prediction (4DVAR, horizontal resolution around 20 km in Antarctica with 105 vertical levels); 2) a computation of singular vectors around Antarctica to identify the regions with the most potential for a rapid forecast error growth, which can be used as an indication where the additional observations should be the best for improving subsequent forecasts; and 3) the nonhydrostatic model AROME (Seity et al. 2011) (1.5-km grid spacing, 90 vertical levels, and initial and lateral boundary conditions from ARPEGE) in near-real time for a large subdomain covering Dome C and Dumont d'Urville (DDU).

From ARPEGE and AROME (Fig. 10), specific output for the YOPPsiteMIIP stations has been produced with the MMDF format for the winter YOPP-SH period. Figure 10b shows the additional number of observations of temperature from sounding data launched at 0600 and 1800 UTC during the TOPs. Figure 11 shows a preliminary comparison of observed and forecast near-surface air temperature at the Dome C Station for the winter YOPP-SH SOP. Model values at 1-h intervals come from daily forecasts starting at 0000 UTC. Both models have a warm bias at 2 m and a cold bias at 40 m. This is typically a signal of excessive mixing near the surface and in the turbulence scheme, suggesting improvements are needed in the model planetary boundary layer schemes for very stable conditions. At 2 m, AROME has a larger warm bias but with a smaller standard deviation. At 40 m, the cold bias is about -4°C for both models. Interestingly, the AROME spatial variability among the 36 closest grid cells is larger at 2 m than at 40 m, even if Dome C is rather homogeneous. In addition, because the standard deviation of the models' errors is significantly larger than the AROME spatial variability, we can conclude that there are no issues with the models' horizontal scale and the observations' spatial representativity.

7. The scarcity of weather services in Antarctica, the Southern Ocean, and sub-Antarctic

Weather information is used every day to plan activities and manage risks to human safety in the Antarctic region (Heinrich and Norris 2024). In addition to being accessible, a weather forecasting process requires accuracy and effectiveness across prediction, communication,

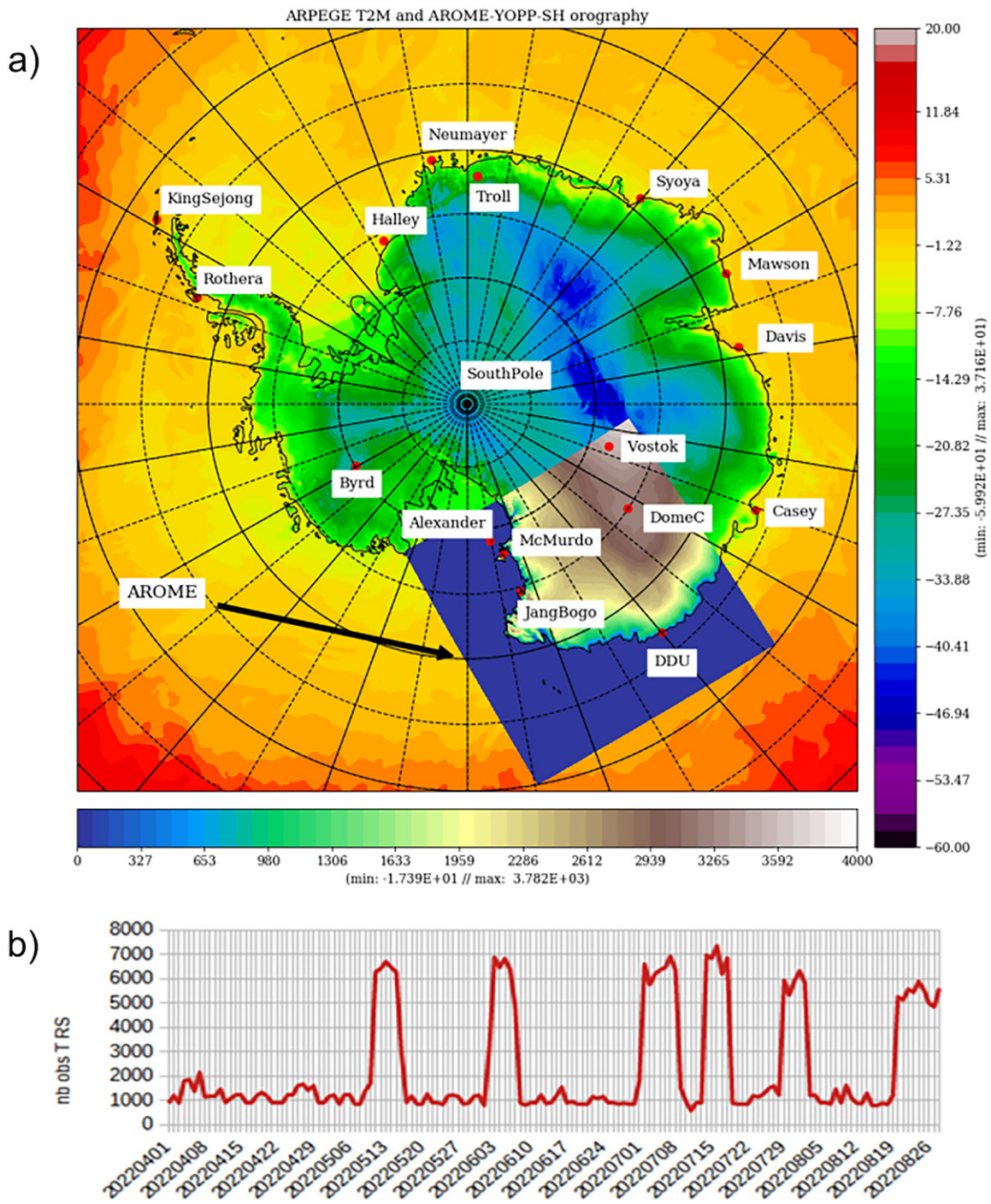


FIG. 10. (a) Stations selected as YOPPsiteMIIP supersites with an example of the ARPEGE model output (for 2-m temperature) and AROME-SH domain and topography; (b) number of temperature observations used in the ARPEGE 4DVAR at 0600 and 1800 UTC during the winter YOPP-SH (courtesy Hervé Benichou Météo-France).

and use, to be successful and realize social benefit and value (Pielke and Carbone 2002; Dawson et al. 2017). However, environmental predictions are less accurate and accessible in the polar regions which, with growing human activity and climate change, increases safety risks (Jung et al. 2016; Jung and Matsueda 2016; Dawson et al. 2017). There is limited empirical research on Antarctic weather information accessibility, use, services, and user needs. Focusing on communication and use, V. Heinrich's mixed-methods Ph.D. study with southern polar weather users (Heinrich and Norris 2024) contributes to our understanding of Antarctic weather information use and decision-making to enhance services and product utility.

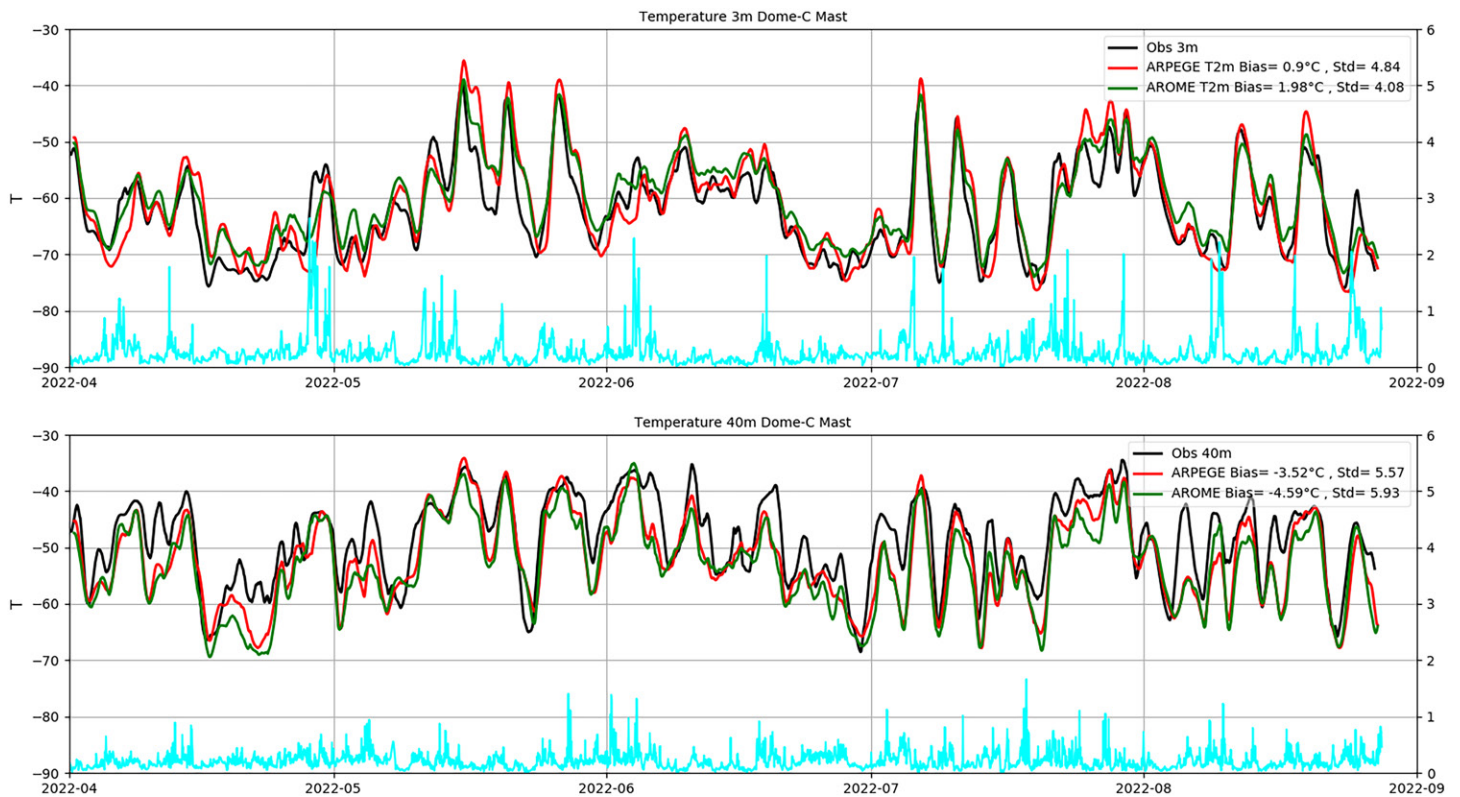


FIG. 11. Time series of hourly temperature at (top) 3 m and (bottom) 40 m above ground from mast observations at Dome C (black lines; data courtesy C. Genthon), the ARPEGE output at the nearest grid point (red lines), and the mean of the 36 nearest grid points of AROME (green line). Blue lines show the AROME standard deviation based on the spatial variability among the 36 grid points (from 1 Apr to 31 Aug 2022).

The study found that 40% of participants engaged by tourism operators did not have access to tailored weather forecasts compared to 4% of those within national Antarctic programs (NAPs; see Fig. 12). Weather service levels vary by organization, accessibility (cost, availability, and bandwidth resources), season, and information provided. At the highest level of service provision, tailored weather services, from collocated onsite meteorologists, assist with interpretation and task prioritization, increasing efficiency and safety. Users outside NAPs and bespoke weather service agreements “make do” with the publicly available information they know about or can access. Publicly available (free) NWP models and forecasts provide less resolution and therefore less information and more uncertainty for decision-makers. Additionally, a generic forecast from a provider may not be fit for the intended purpose in terms of the format or in providing the information and actionable knowledge needed to support all users’ decision-making across their varied goals and activities (Morss et al. 2008, 2005; Pielke

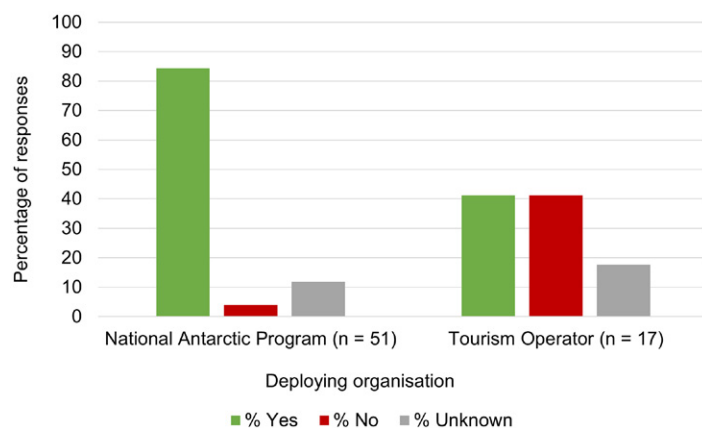


FIG. 12. Responses (yes, no, and unknown) to the question of did participants ($N = 62$) have access to forecasts from a forecaster, meteorologist, or other weather professional when deployed to the Antarctic and/or sub-Antarctic? Some participants had worked for NAPs and tourism operators during their polar careers.

and Carbone 2002). Thus, users reliant on freely available models and generic forecasts use poorer quality information that is not tailored to their decision-making contexts, activities, or locations. These users have less clarity and greater uncertainty and risk in their Antarctic planning, decision-making, and activities. More research is needed, but limited weather services and a mismatch with user needs may help explain the diversity of information sources listed by survey participants and the popularity of websites like [windy.com](https://www.windy.com) (Heinrich and Norris 2024; Heinrich et al. 2024). There is a gap in Antarctic weather service provision for users who do not have access to tailored or commercial services, and in the information, accuracy, timeliness, resolution, and contextual detail needed to support everyday activities across all sectors. Insufficient weather services in Antarctic and Southern Ocean regions increase risks to safety in human activities.

8. SIPN South

For the SOP, a dedicated Antarctic sea ice prediction experiment was devised. The experiment followed the usual SIPN South project protocol (see Massonnet et al. 2023) except that the initialization date was set to 1 May (and not 1 December as usual). Forecasts were collected from eight groups that used either coupled climate modeling approaches or statistical approaches. The forecasts were received in real conditions, i.e., before 1 May 2022. The groups were asked to provide diagnostics of daily sea ice area and concentration for the period 1 May–31 August 2022.

A comparison between the SIPN South forecasts and the verifying observations (Fig. 13) reveals the existence of two subgroups. The first subgroup, comprising the SINTEX-F2 and Université Catholique de Louvain (ucl) contributions, features a high bias in sea ice area of about +35% compared to observations at the end of the SOP. It is noteworthy that both contributions are generated with dynamical process-based models. For the ucl forecast, this bias is already present at the initialization time and can be explained by the lack of data assimilation in that model or by biases in the atmospheric reanalyses driving the model.

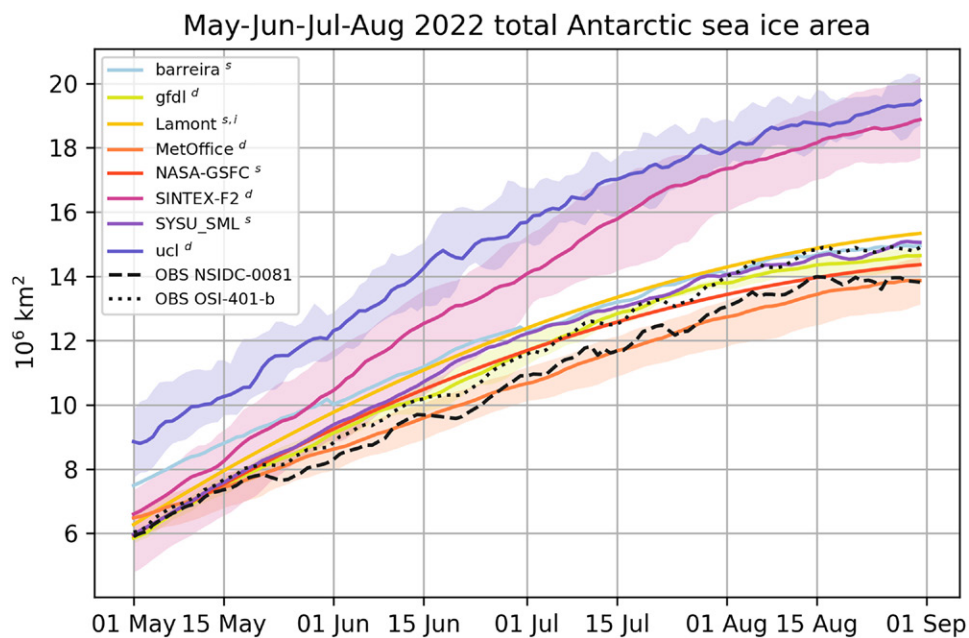


FIG. 13. Temporal evolution of the total Antarctic sea ice area forecasted by eight groups and institutions participating in the SOP 2022 SIPN South experiment. The thick colored lines denote the forecast ENS median, while the shadings denote the ENS ranges. The letters *s* and *d* in the legend refer to forecasts produced with statistical and dynamical models, respectively. The letter *i* expresses that the output has been interpolated (quadratically) from monthly to daily values. The two broken lines are observed sea ice areas from two satellite datasets.

For the SINTEX-F2 forecast, the bias develops over time, suggesting that the benefits of initialization are progressively overridden by the model's systematic biases. The second subgroup, comprising four statistical models (Barreira, NASA-GSFC, Lamont, and SYSU_SML) and two dynamical climate models (GFDL and Met Office), appears to simulate the seasonal development of the Antarctic sea ice area rather well. It is worth mentioning that the observed sea ice area seasonal cycle remained well below the long-term climatology throughout 2022. This second subgroup thus represents some added value, from a prediction point of view, over a naive climatological forecast that would have overestimated the actual sea ice evolution.

The results of this autumn–winter experiment can be compared to the results of the summer experiments that have been coordinated since 2017 through the SIPN South project. In the summer predictions, a large spread exists at the initial time (1 December) and the spread remains appreciable in February (see Massonnet et al. 2023) even within statistical contributions. Previous works have suggested that the inherent predictability of sea ice extent is much more limited for the summer season than for the winter season (Chevallier et al. 2019). For the autumn–winter season, several studies have highlighted the potential predictability of sea ice anomalies, thanks to the memory-holding capacity of the subsurface ocean (Marchi et al. 2019; Holland et al. 2013), a mechanism that is less active in summer. Moreover, a recent modeling study (Goosse et al. 2023) has suggested that the seasonal advance of sea ice in autumn and winter is mostly controlled by two factors, namely, the initial summer sea ice extent and the insolation; in contrast, the seasonal retreat in spring and summer is controlled by additional atmospheric and oceanic feedbacks, which could explain why it is more difficult to predict summer conditions than winter ones.

9. Conclusions

The successful use of the targeted observing period (TOP) strategy has been described as a means to study and improve numerical weather prediction (NWP) accuracy during the austral winter over the Southern Ocean and Antarctica. It is based upon the release of additional radiosonde balloons during seven TOPs of 5–10-day duration each, more than doubling the routine sounding program at the 24 participating stations run by 14 national Antarctic programs. These data are actively being evaluated for their impact on forecast skill via data denial experiments with the goal of refining the observing system to improve NWP for winter conditions that are becoming steadily more important for Antarctic science and operations. In addition, extensive observations focusing on clouds and precipitation primarily during ARs are being applied to refine model microphysical parameterizations for the ubiquitous mixed-phase clouds that frequently impact coastal Antarctica. Model physics investigations are currently being facilitated by high-temporal-resolution observations and model output at the YOPPSiteMIIP supersites.

Parallel investigations are broadening the scope and impact of YOPP-SH winter SOP. Studies of the Antarctic tourist industry's use of weather forecasts show the scope for much greater awareness of the availability of forecast products and the skill they exhibit. Conversely, tailoring the weather information for this group of users would further incorporate the recently advanced forecast skill. There is also the prospect of the tourist industry being actively engaged in better forecast delivery by providing observations of current weather conditions. The SIPN South analysis of projections of the sea ice growth period reveals that the forecast skill several months ahead is superior to that of the sea ice contraction phase.

Until now, the YOPP-SH investigations have had little direct impact on the practices of the global forecasting centers; i.e., the research to operations (RTO) connection is yet to be realized. The Polar Coupled Analysis and Prediction for Services (PCAPS) program intends to address this shortcoming by engaging with ECMWF, the Australian Bureau of Meteorology,

the National Weather Service of Argentina, and probably additional global weather centers. PCAPS is a new initiative of the World Weather Research Program of the World Meteorological Organization to follow on from the Polar Prediction Project and focuses on coupled atmosphere–ocean–sea ice analysis and modeling. It is slated to span 2024–28 with a major emphasis on service delivery.

Acknowledgments. Preparation of this manuscript, that is, contribution 1628 of Byrd Polar and Climate Research Center, was supported in part by NSF Grant 2205398. The Scientific Committee for Antarctic Research (SCAR) through its Physical Sciences Group funded the publication charges. We are grateful for all observers at the stations who volunteered to prepare and release the additional TOP radiosondes. The creation of the polar AR toolkit was supported by NSF Grants 2127632 and 2229392. Polar WRF simulations of ARs were performed on the San Diego Supercomputing Center’s COMET with support provided by the California AR Program, Phase II 460001361 and Phase III 4600014294 (State of California, Department of Water Resources). We thank ECMWF for making available high-resolution forecast products during the winter YOPP-SH period and ERA5 reanalysis data (available via Copernicus Climate Change Service; <https://cds.climate.copernicus.eu>). Enhanced radiosonde observations during winter YOPP-SH in the Antarctic Peninsula–Weddell Sea region were possible, thanks to the support by Chilean Weather Service (DMC), Chilean Antarctic Institute (INACH Grant RT_69-20), and Chilean Science Agency (ANILLO Grant ACT210046 and FONDECYT 1221122) at Escudero; Korea Polar Research Institute (KOPRI, PE23030) at King Sejong; Servicio Meteorológico Nacional (SMN) and Dirección Nacional del Antártico (DNA), Argentina, Marambio; and National Antarctic Scientific Center (NASC) of Ukraine at Vernadsky. Deployment of the MRR2 radar at the Escudero Station was supported by the Institut des Géosciences de l’Environnement (CNRS, France) via collaboration with Vincent Favier. Météo-France and Institut polaire français Paul-Emile Victor (IPEV) supported extra radiosonde releases at Kerguelen and Dumont d’Urville. IVG thanks the support by the strategic funding to CIIMAR (UIDB/04423/2020, UIDP/04423/2020); CESAM (UIDP/50017/2020, UIDB/50017/2020, and LA/P/0094/2020); 2021.03140.CEECIND; project ATLACE (CIRCNA/CAC/0273/2019); and Portuguese Polar Program through national funds provided by Fundação para a Ciência e a Tecnologia (FCT). SK and AC were supported by the Ukrainian State Special-Purpose Research Program in Antarctica for 2011–23. JDW acknowledges the support from the Agence Nationale de la Recherche project ANR-20-CE01-0013 (ARCA). We are grateful to Robert Stillwell for help with analysis and interpretation of MPL results at Escudero, to Peter Kuma for the open-source `mpl2nc` codebase to convert MPL data to netcdf format (<https://github.com/peterkuma/mpl2nc>), and to Barbara Casati (Environment and Climate Change Canada) for helping to link YOPP-SH with YOPPsiteMIIP and providing an example of MMDF output. Deployment of the instrumentation to Davis, the ongoing operation of the VHF radar, and the contributions of S. P. Alexander and W. J. R. French to this project were supported by the Australian Antarctic Division through Australian Antarctic Science projects 4387, 4445, and 4637. We thank Derryn Harvie for his invaluable assistance in installing, commissioning, and maintaining the instruments at Davis throughout 2022. We thank the Australian Bureau of Meteorology staff and forecasters who helped coordinate the TOPs and the technical officers at the eight meteorological observing offices who supported this work through additional radiosonde launches. Thanks to David Mikolajczyk, Matthew G. Noojin, Ethan Koudelka, Bella Onsi, Anastasia Tomanek, and Karissa Shannon for their help with the data repository efforts at the Antarctic Meteorological Research and Data Center (AMRDC) along with support from NSF Grants 1951720 and 1951603. We appreciate the contributions of the three anonymous reviewers toward improving the clarity of the manuscript.

Data availability statement. The YOPP-SH data repository collection can be found at <https://amrdcdata.ssec.wisc.edu/group/year-of-polar-prediction-in-the-southern-hemisphere>. The corresponding author will also aid in locating and accessing YOPP-SH datasets from the winter TOPs, bromwich.1@osu.edu.

References

- Alexander, S. P., A. Orr, S. Webster, and D. J. Murphy, 2017: Observations and fine-scale model simulations of gravity waves over Davis, East Antarctica (69°S, 78°E). *J. Geophys. Res. Atmos.*, **122**, 7355–7370, <https://doi.org/10.1002/2017JD026615>.
- , G. M. McFarquhar, R. Marchand, A. Protat, É. Vignon, G. G. Mace, and A. R. Klekociuk, 2021: Mixed-phase clouds and precipitation in Southern Ocean cyclones and cloud systems observed poleward of 64°S by ship-based cloud radar and lidar. *J. Geophys. Res. Atmos.*, **126**, e2020JD033626, <https://doi.org/10.1029/2020JD033626>.
- , A. Protat, A. Berne, and L. Ackermann, 2023: Radar-derived snowfall microphysical properties at Davis, Antarctica. *J. Geophys. Res. Atmos.*, **128**, e2022JD038389, <https://doi.org/10.1029/2022JD038389>.
- Bromwich, D. H., D. F. Steinhoff, I. Simmonds, K. Keay, and R. L. Fogt, 2011: Climatological aspects of cyclogenesis near Adelie Land Antarctica. *Tellus*, **63A**, 921–938, <https://doi.org/10.1111/j.1600-0870.2011.00537.x>.
- , and Coauthors, 2020: The Year of Polar Prediction in the Southern Hemisphere (YOPP-SH). *Bull. Amer. Meteor. Soc.*, **101**, E1653–E1676, <https://doi.org/10.1175/BAMS-D-19-0255.1>.
- , J. G. Powers, K. W. Manning, and X. Zou, 2022: Antarctic data impact experiments with Polar WRF during the YOPP-SH summer special observing period. *Quart. J. Roy. Meteor. Soc.*, **148**, 2194–2218, <https://doi.org/10.1002/qj.4298>.
- Chen, S.-Y., T.-K. Wee, Y.-H. Kuo, and D. H. Bromwich, 2014: An impact assessment of GPS radio occultation data on prediction of a rapidly developing cyclone over the Southern Ocean. *Mon. Wea. Rev.*, **142**, 4187–4206, <https://doi.org/10.1175/MWR-D-14-00024.1>.
- Chevallier, M., F. Massonnet, H. Goessling, V. Guémas, and T. Jung, 2019: The role of sea ice in sub-seasonal predictability. *Sub-Seasonal to Seasonal Prediction*, A. W. Robertson and F. Vitart, Eds., Elsevier, 201–221, <https://doi.org/10.1016/B978-0-12-811714-9.00010-3>.
- Choi, Y., S.-J. Kim, D. H. Bromwich, J. G. Powers, H. Kwon, and S.-J. Park, 2023: Effects of assimilation of YOPP-SH additional radiosonde observations on analyses and forecasts over Antarctica in austral summer. *Quart. J. Roy. Meteor. Soc.*, **149**, 2719–2741, <https://doi.org/10.1002/qj.4528>.
- Dawson, J., and Coauthors, 2017: Navigating weather, water, ice and climate information for safe polar mobilities. WWRP/PPP. 5 - 2017, World Meteorological Organization, 84 pp., https://epic.awi.de/id/eprint/462111/012_WWRP_PPP_No_5_2017_11_OCT.pdf.
- Ferrone, A., A. C. Billault-Roux, and A. Berne, 2022: ERUO: A spectral processing routine for the Micro Rain Radar PRO (MRR-PRO). *Atmos. Meas. Tech.*, **15**, 3569–3592, <https://doi.org/10.5194/amt-15-3569-2022>.
- Gehring, J., É. Vignon, A.-C. Billault-Roux, A. Ferrone, A. Protat, S. P. Alexander, and A. Berne, 2022: Orographic flow influence on precipitation during an atmospheric river event at Davis, Antarctica. *J. Geophys. Res. Atmos.*, **127**, e2021JD035210, <https://doi.org/10.1029/2021JD035210>.
- Gonzalez, S., A. Callado, M. Martínez, and B. Elvira, 2020: The AEMET-γSREPS over the Antarctic Peninsula and the impact of kilometer-resolution EPS on logistic activities on the continent. *Adv. Sci. Res.*, **17**, 209–217, <https://doi.org/10.5194/asr-17-209-2020>.
- Goosse, H., and Coauthors, 2023: Modulation of the seasonal cycle of the Antarctic sea ice extent by sea ice processes and feedbacks with the ocean and the atmosphere. *Cryosphere*, **17**, 407–425, <https://doi.org/10.5194/tc-17-407-2023>.
- Gorodetskaya, I. V., and Coauthors, 2023: Record-high Antarctic Peninsula temperatures and surface melt in February 2022: A compound event with an intense atmospheric river. *njp Climate Atmos. Sci.*, **6**, 202, <https://doi.org/10.1038/s41612-023-00529-6>.
- Guyot, A., A. Protat, S. P. Alexander, A. R. Klekociuk, P. Kuma, and A. McDonald, 2022: Detection of supercooled liquid water containing clouds with ceilometers: Development and evaluation of deterministic and data-driven retrievals. *Atmos. Meas. Tech.*, **15**, 3663–3681, <https://doi.org/10.5194/amt-15-3663-2022>.
- Heinrich, V. J., and K. Norris, 2024: Situational awareness and safety: Using weather information to inform decision-making in Antarctic environments. *Wea. Climate Soc.*, <https://doi.org/10.1175/WCAS-D-23-0125.1>, in press.
- , and Coauthors, 2024: The use of weather, water, ice, and climate (WWIC) information in the polar regions: What is known after the decade-long Polar Prediction Project? *Wea. Climate Soc.*, **16**, 369–387, <https://doi.org/10.1175/WCAS-D-23-0105.1>.
- Holland, M. M., E. Blanchard-Wrigglesworth, J. Kay, and S. Vavrus, 2013: Initial-value predictability of Antarctic sea ice in the Community Climate System Model 3. *Geophys. Res. Lett.*, **40**, 2121–2124, <https://doi.org/10.1002/grl.50410>.
- Hoskins, B. J., and K. I. Hodges, 2005: A new perspective on Southern Hemisphere storm tracks. *J. Climate*, **18**, 4108–4129, <https://doi.org/10.1175/JCLI3570.1>.
- Jung, T., and M. Matsueda, 2016: Verification of global numerical weather forecasting systems in polar regions using TIGGE data. *Quart. J. Roy. Meteor. Soc.*, **142**, 574–582, <https://doi.org/10.1002/qj.2437>.
- , and Coauthors, 2016: Advancing polar prediction capabilities on daily to seasonal time scales. *Bull. Amer. Meteor. Soc.*, **97**, 1631–1647, <https://doi.org/10.1175/BAMS-D-14-00246.1>.
- Kulie, M. S., and R. Bennartz, 2009: Utilizing spaceborne radars to retrieve dry snowfall. *J. Appl. Meteor. Climatol.*, **48**, 2564–2580, <https://doi.org/10.1175/2009JAMC2193.1>.
- Lewis, J. R., J. R. Campbell, E. J. Welton, S. A. Stewart, and P. C. Haftings, 2016: Overview of MPLNET version 3 cloud detection. *J. Atmos. Oceanic Technol.*, **33**, 2113–2134, <https://doi.org/10.1175/JTECH-D-15-0190.1>.
- Liu, Z., J. Ban, J.-S. Hong, and Y.-H. Kuo, 2020: Multi-resolution incremental 4D-Var for WRF: Implementation and application at convective scale. *Quart. J. Roy. Meteor. Soc.*, **146**, 3661–3674, <https://doi.org/10.1002/qj.3865>.
- Marchi, S., T. Fichefet, H. Goosse, V. Zunz, S. Tietsche, J. J. Day, and E. Hawkins, 2019: Reemergence of Antarctic sea ice predictability and its link to deep ocean mixing in global climate models. *Climate Dyn.*, **52**, 2775–2797, <https://doi.org/10.1007/s00382-018-4292-2>.
- Massonnet, F., and Coauthors, 2023: SIPN South: Six years of coordinated seasonal Antarctic sea ice predictions. *Front. Mar. Sci.*, **10**, 1148899, <https://doi.org/10.3389/fmars.2023.1148899>.
- Morss, R. E., O. V. Wilhelmi, M. W. Downton, and E. Grunfest, 2005: Flood risk, uncertainty, and scientific information for decision making: Lessons from an interdisciplinary project. *Bull. Amer. Meteor. Soc.*, **86**, 1593–1602, <https://doi.org/10.1175/BAMS-86-11-1593>.
- , J. K. Lazo, B. G. Brown, H. E. Brooks, P. T. Ganderton, and B. N. Mills, 2008: Societal and economic research and applications for weather forecasts: Priorities for the North American THORPEX program. *Bull. Amer. Meteor. Soc.*, **89**, 335–346, <https://doi.org/10.1175/BAMS-89-3-335>.
- O'Connor, E. J., A. J. Illingworth, and R. J. Hogan, 2004: A technique for autocalibration of cloud lidar. *J. Atmos. Oceanic Technol.*, **21**, 777–786, [https://doi.org/10.1175/1520-0426\(2004\)021<0777:ATFAOC>2.0.CO;2](https://doi.org/10.1175/1520-0426(2004)021<0777:ATFAOC>2.0.CO;2).
- Peters, G., B. Fischer, and M. Clemens, 2010: Rain attenuation of radar echoes considering finite-range resolution and using drop size distributions. *J. Atmos. Oceanic Technol.*, **27**, 829–842, <https://doi.org/10.1175/2009JTECHA1342.1>.
- Pielke, R., Jr., and R. E. Carbone, 2002: Weather impacts, forecasts, and policy: An integrated perspective. *Bull. Amer. Meteor. Soc.*, **83**, 393–406, [https://doi.org/10.1175/1520-0477\(2002\)083<0393:WIFAP>2.3.CO;2](https://doi.org/10.1175/1520-0477(2002)083<0393:WIFAP>2.3.CO;2).
- Ralph, F. M., J. J. Rutz, J. M. Cordeira, M. Dettinger, M. Anderson, D. Reynolds, L. J. Schick, and C. Smallcomb, 2019: A scale to characterize the strength and impacts of atmospheric rivers. *Bull. Amer. Meteor. Soc.*, **100**, 269–289, <https://doi.org/10.1175/BAMS-D-18-0023.1>.
- Seity, Y., P. Brousseau, S. Malardel, G. Hello, P. Bénard, F. Bouttier, C. Lac, and V. Masson, 2011: The AROME-France convective-scale operational model. *Mon. Wea. Rev.*, **139**, 976–991, <https://doi.org/10.1175/2010MWR3425.1>.

- Simmons, A. J., and A. Hollingsworth, 2002: Some aspects of the improvement in skill of numerical weather prediction. *Quart. J. Roy. Meteor. Soc.*, **128**, 647–677, <https://doi.org/10.1256/003590002321042135>.
- Skamarock, W. C., and Coauthors, 2019: A description of the Advanced Research WRF Model version 4.1. NCAR Tech. Note NCAR/TN-556+STR, 145 pp., <https://doi.org/10.5065/1dfh-6p97>.
- Stillwell, R. A., R. R. Neely III, J. P. Thayer, M. D. Shupe, and D. D. Turner, 2018: Improved cloud-phase determination of low-level liquid and mixed-phase clouds by enhanced polarimetric lidar. *Atmos. Meas. Tech.*, **11**, 835–859, <https://doi.org/10.5194/amt-11-835-2018>.
- Svensson, G., and Coauthors, 2023: Warm air intrusions reaching the MOSAiC expedition in April 2020—The YOPP targeted observing period (TOP). *Elementa*, **11**, 00016, <https://doi.org/10.1525/elementa.2023.00016>.
- Wang, X., D. M. Barker, C. Snyder, and T. M. Hamill, 2008: A hybrid ETKF–3DVAR data assimilation scheme for the WRF model. Part II: Real observation experiments. *Mon. Wea. Rev.*, **136**, 5132–5147, <https://doi.org/10.1175/2008MWR2445.1>.
- Wille, J. D., V. Favier, A. Dufour, I. V. Gorodetskaya, J. Turner, C. Agosta, and F. Codron, 2019: West Antarctic surface melt triggered by atmospheric rivers. *Nat. Geosci.*, **12**, 911–916, <https://doi.org/10.1038/s41561-019-0460-1>.
- , and Coauthors, 2021: Antarctic atmospheric river climatology and precipitation impacts. *J. Geophys. Res. Atmos.*, **126**, e2020JD033788, <https://doi.org/10.1029/2020JD033788>.
- , and Coauthors, 2022: Intense atmospheric rivers can weaken ice shelf stability at the Antarctic Peninsula. *Commun. Earth Environ.*, **3**, 90, <https://doi.org/10.1038/s43247-022-00422-9>.
- , and Coauthors, 2024a: The extraordinary March 2022 East Antarctic “heat” wave. Part I: Observations and meteorological drivers. *J. Climate*, **37**, 757–778, <https://doi.org/10.1175/JCLI-D-23-0175.1>.
- , and Coauthors, 2024b: The extraordinary March 2022 East Antarctic “heat” wave. Part II: Impacts on the Antarctic ice sheet. *J. Climate*, **37**, 779–799, <https://doi.org/10.1175/JCLI-D-23-0176.1>.
- Zou, X., and Coauthors, 2023: Strong warming over the Antarctic Peninsula during combined atmospheric river and foehn events: Contribution of shortwave radiation and turbulence. *J. Geophys. Res. Atmos.*, **128**, e2022JD038138, <https://doi.org/10.1029/2022JD038138>.
- Zsoter, E., 2006: Recent developments in extreme weather forecasting. *ECMWF Newsletter*, No. 107, ECMWF, Reading, United Kingdom, 8–17, <https://www.ecmwf.int/en/eLibrary/80443-recent-developments-extreme-weather-forecasting>.